Acta Crystallographica Section D
Biological Crystallography
ISSN 0907-4449

Structures of the PKC-ι kinase domain in its ATP-bound and apo forms reveal defined structures of residues 533–551 in the C-terminal tail and their roles in ATP binding

Tetsuo Takimura,* Kenji Kamata, Kazuhiro Fukasawa, Hirokazu Ohsawa, Hideya Komatani, Takashi Yoshizumi, Ikuko Takahashi, Hidehito Kotani and Yoshikazu Iwasawa

Tsukuba Research Institute, Merck Research Laboratories, Banyu Pharmaceutical Co. Ltd, Okubo-3, Tsukuba, 300-2611 Ibaraki, Japan

Correspondence e-mail: tetsuo_takimura@merck.com

Received 1 November 2009
Accepted 10 February 2010

PDB References: PKC-ι, ATP complex, 3a8w; apo form, 3a8x.

Protein kinase C (PKC) plays an essential role in a wide range of cellular functions. Although crystal structures of the PKC-θ, PKC-ι and PKC-βII kinase domains have previously been determined in complexes with small-molecule inhibitors, no structure of a PKC–substrate complex has been determined. In the previously determined PKC-ι complex, residues 533–551 in the C-terminal tail were disordered. In the present study, crystal structures of the PKC-ι kinase domain in its ATP-bound and apo forms were determined at 2.1 and 2.0 Å resolution, respectively. In the ATP complex, the electron density of all of the C-terminal tail residues was well defined. In the structure, the side chain of Phe543 protrudes into the ATP-binding pocket to make van der Waals interactions with the adenine moiety of ATP; this is also observed in other AGC kinase structures such as binary and ternary substrate complexes of PKA and AKT. In addition to this interaction, the newly defined residues around the turn motif make multiple hydrogen bonds to glycine-rich-loop residues. These interactions reduce the flexibility of the glycine-rich loop, which is organized for ATP binding, and the resulting structure promotes an ATP conformation that is suitable for the subsequent phosphoryl transfer. In the case of the apo form, the structure and interaction mode of the C-terminal tail of PKC-ι are essentially identical to those of the ATP complex. These results indicate that the protein structure is pre-organized before substrate binding to PKC-ι, which is different from the case of the prototypical AGC-branch kinase PKA.

1. Introduction

Protein kinases C constitute a family of Ser/Thr kinases that belong to the AGC branch (Manning *et al.*, 2002) and are subdivided into conventional (PKC-α, PKC-βI, PKC-βII and PKC-γ), novel (PKC-δ, PKC-ε, PKC-θ and PKC-η) and atypical (PKC-ζ, PKC-ι/λ and PKC-μ) isoforms depending on their regulatory-domain structures and cofactor requirements (Tan & Parker, 2003). Atypical PKCs, which require phosphatidylserine, contain a PB1 domain and an atypical C1 domain. Atypical PKCs play important roles in controlling cell growth and survival (see Moscat & Diaz-Meco, 2000, and references therein) and PKC-ι has been proposed to be an attractive target for the development of novel therapeutics against colon cancer and chronic myelogenous leukaemia (Gustafson *et al.*, 2004).

A structure is currently available for each subfamily of the PKC family, *e.g.* the PKC-βII–bisindolylmaleimide-2 (BIM2) complex for the conventional PKCs (Grodsky *et al.*, 2006), the PKC-θ–staurosporine complex for the novel PKCs (Xu *et al.*, 2004) and the PKC-ι–bisindolylmaleimide-1 (BIM1) complex for the atypical PKCs (Messerschmidt *et al.*, 2005). In addition to these PKCs, structures of many other AGC-branch kinases have been determined. Among these, the structures of cAMP-dependent protein kinase (PKA) have been most investigated; it was the first kinase for which the structure was determined. Subsequently, structures of the apo form, binary and ternary substrate complexes and many inhibitor complexes have also been determined (see Taylor *et al.*, 2004 and references therein). Therefore, PKA is the prototypical model for the structural biology of AGC-branch kinases.

Multiple AGC-branch kinases have a C-terminal tail region after their kinase core (Gold *et al.*, 2006). In this region, a hydrophobic motif (HM; F*XX*FS/T) is conserved in many AGC-branch kinases and phosphorylation of the Thr/Ser in the HM is important for activation. In the case of PKC-ι the last residue of the HM is replaced by Glu, which mimics phospho-Ser or phospho-Thr (pSer or pThr), and the interaction mode of the HM is similar to those in other AGC kinases. In addition to the HM, there is another phosphorylation site (turn motif) in the C-terminal tails of PKC, AKT/PKB and PKA. Although these residues are conserved at the sequence level, crystal structures have revealed different interaction modes in these three kinases. In the PKC-ι–BIM1 complex pThr makes hydrogen bonds to two basic residues from the β3 and β5 strands in the small lobe of the kinase core, while in the PKA binary and ternary substrate complexes pSer makes hydrogen bonds to neighbouring residues in the sequence and the motif in ATK/PKB is disordered.

Considerable insights into the C-terminal tail region have been obtained from the previously determined PKC-ι–BIM1 complexes; however, the region contains unobserved residues between 533 and 551, the roles of which remain unknown. In addition, no structure of a substrate complex of the PKC-family kinases has been determined.

In this report, we report the structures of an ATP complex and the apo form of PKC-ι. In these structures the residues in the C-terminal tail region that were disordered in the previously determined BIM1 complex are clearly defined and their role in activation will be discussed.

2. Experimental procedures

Complete EDTA-free was purchased from Roche Diagnostics K.K. The vectors pFastBacHTa and pENTR D-Topo and TEV protease were purchased from Invitrogen Japan K.K. HisTrap HP, MonoQ 10/100 GL and HiLoad 16/60 Superdex 200 pg were purchased from GE Healthcare. An Advantec Dismic 25cs syringe filter with a pore size of 0.20 µm was used. Proteins were concentrated using Amicon Ultra-4, 10 000 molecular-weight cutoff (Millipore). The Seeding Tool from Hampton Research was used for streak-seeding.

2.1. Preparation of the expression construct

For the preparation of the expression construct, cDNA fragments for the His-tag/TEV part and for the human PKC-ι kinase domain (240–579) were cloned into cloning vectors individually and the two cDNA fragments were then ligated into an expression vector for the fused protein. For the N-terminal His-tag/TEV protease site, a cDNA with an attached *Bam*HI site at the 5′ end was amplified by PCR from the initiation codon to the SV40 polyadenylation signal in pFastBacHTa. In this region, there is one *Nco*I site just after the TEV recognition site. For human PKC-ι (240–579) (SwissProt P41743), a cDNA with *Nco*I and *Xho*I sites at the 5′ and 3′ ends, respectively, was amplified by PCR. The cDNA fragments were cloned individually into a cloning vector (pENTR D-Topo). The fragment containing the His tag and TEV protease site was digested by *Bam*HI and *Nco*I and another fragment for PKC-ι (240–579) was digested with *Nco*I and *Xho*I. These two fragments were ligated into pBacPak9 using *Bam*HI and *Xho*I sites, resulting in a fusion protein consisting of PKC-ι (240–579) with an N-terminal His tag and TEV cleavage site.

2.2. Expression and purification of protein

Recombinant baculoviruses were obtained using standard procedures. For expression, Sf9 cells were infected by the recombinant baculoviruses and cells were harvested after 3 d incubation at 301 K. The cells were frozen and stored at 193 K.

Cells were suspended in lysis buffer [20 m*M* sodium phosphate pH 7.4, 500 m*M* NaCl, 20 m*M* imidazole, 5% glycerol, 1% Triton X-100, 5 m*M* 2-mercaptoethanol, Complete EDTA-free (one tablet per 50 ml of buffer), 50 m*M* sodium fluoride] and homogenized by sonication. The suspension was centrifuged at 20 000*g*. The lysate was filtrated by a 0.20 µm syringe filter and loaded onto a HisTrap HP column equilibrated with buffer *A* (20 m*M* sodium phosphate pH 7.4, 500 m*M* NaCl, 20 m*M* imidazole, 5% glycerol, 5 m*M* 2-mercaptoethanol). The column was washed with buffer *A* and 5% buffer *B* (the same as buffer *A* except that the imidazole concentration was 500 m*M*). Protein was eluted with a linear gradient from 5% to 100% buffer *B*. Pooled fractions were concentrated and the His tag was cleaved off by TEV protease at 277 K overnight according to the manufacturer's instructions. The incubated solution was dialyzed against buffer *A*. The solution was loaded onto a HisTrap HP column (5 ml) equilibrated with buffer *A* and the flowthrough fractions were collected. The protein solution was then loaded onto a MonoQ 10/100 GL anion-exchange column equilibrated with buffer *C* (25 m*M* sodium citrate pH 6.0, 50 m*M* NaCl, 0.5 m*M* EDTA, 5% glycerol, 2 m*M* DTT) followed by elution with a 100% NaCl gradient to buffer *D* (the same as buffer *C* except that the NaCl concentration was 500 m*M*).

For phosphorylation of Thr403 in the activation loop, the protein was concentrated to 1 mg ml^{-1} by ultracentrifugation and buffer-exchanged to buffer *E* (20 m*M* Tris pH 7.5, 15 m*M* $MgCl_2$, 1 m*M* EGTA, 2 m*M* DTT). The protein was then

Table 1
Diffraction statistics of the ATP complex and the apo form.

Values in parentheses are for the last shell.

	ATP complex	Apo form
Space group	$C222_1$	$C222_1$
Unit-cell parameters (Å, °)	a = 85.04, b = 89.14, c = 206.40, $\alpha = \beta = \gamma = 90$	a = 84.90, b = 89.15, c = 204.27, $\alpha = \beta = \gamma = 90$
Resolution (Å)	2.1 (2.18–2.10)	2.0 (2.07–2.00)
Completeness (%)	99.9 (99.9)	92.1 (99.1)
$R_{\rm merge}$ (%)	5.8 (24.0)	7.5 (17.8)
$\langle I/\sigma(I)\rangle$	28.7 (8.1)	18.8 (8.2)
Redundancy	7.1 (6.7)	6.6 (4.8)

incubated with ATP (1 m*M*) and PDK1 (15 ng µl^{-1}) at 293 K for 2 h.

The reaction mixture was loaded onto a MonoQ 10/100 GL column using the same buffer system. The original peak of the unphosphorylated protein completely disappeared and a new peak with a longer retention time appeared. Fractions of the new peak were collected and loaded onto a HiLoad 16/60 Superdex 200 pg column equilibrated with buffer *E* (20 m*M* Tris pH 7.5, 150 m*M* NaCl, 5 m*M* DTT). Dynamic light-scattering analysis showed a monodisperse protein with the molecular weight of the monomeric protein (∼40 000 Da). The protein solution was concentrated to 6–10 mg ml^{-1}. The sample was then flash-frozen in liquid nitrogen and stored at 193 K.

2.3. Crystallization, data collection and structure determination

Crystals of the ATP complex were obtained at 288–293 K by vapour diffusion from hanging drops consisting of 1 µl protein solution containing 5 m*M* ATP and 1 µl reservoir solution (0.1 *M* bis-tris pH 5.5, 0.2 *M* ammonium sulfate, 25–30% PEG 3350). For data collection, a crystal was transferred to cryo-solution (15% glycerol in mother liquor) and frozen in liquid nitrogen. Crystals of the apoenzyme were grown using a similar procedure but with a different reservoir solution (0.1 *M* HEPES pH 7.5, 2% PEG 400, 2.0–2.5 *M* ammonium sulfate). For data collection, a crystal was directly frozen from the drop in liquid nitrogen.

Diffraction data for the ATP complex and the apoenzyme were collected at PF AR-NW12A using an ADSC Quantum 210r CCD detector and PF BL-5A using an ADSC Quantum 315r CCD detector, respectively. The data sets were indexed, integrated and scaled using *HKL*-2000. Crystallographic data-collection and reduction statistics are summarized in Table 1.

The structures were solved by molecular replacement using *Phaser* (McCoy *et al.*, 2005) from the *CCP*4 program suite. The protein part of the PKC-ι–BIM1 complex (PDB code 1zrz; Messerschmidt *et al.*, 2005) was used as a search model. Refinement was performed with *CNX* and *REFMAC*5 (Murshudov *et al.*, 1997). Electron density was clearly observed for residues 533–551 which were disordered in the starting model. For the ATP complex, ligand electron density was also clearly observed in the ATP-binding pocket. These residues and ATP were constructed manually using *Coot* (Emsley & Cowtan, 2004). Additional cycles of refinement were performed with solvent. The final crystallographic refinement statistics are summarized in Table 2.

Table 2
Refinement results of the ATP complex and the apo form.

	ATP complex	Apo form
Resolution range (Å)	50.0–2.1	50.0–2.0
No. of reflections	46144	48414
Completeness (working + test set) (%)	99.9	91.9
R value (working set) (%)	24.7	22.3
Free R value (5.1% test set) (%)	30.1	27.1
No. of atoms	5598	5651
Protein	5369	5442
ATP	62	—
Ions	5	20
Waters	162	189
R.m.s.d. from ideal		
Bond lengths (Å)	0.010	0.006
Bond angles (°)	1.286	0.878
B factor, all atoms (Å^2)	32.5	37.9

3. Results and discussion

3.1. Preparation of crystals

Although the crystal structure of the PKC-ι kinase domain containing residues 224–587 had been determined previously, the resolution was not suitable for a detailed investigation of the structure. Therefore, we tried to improve the quality of the crystal. For this purpose, we paid attention to sequence differences and the length of the constructs for crystallization.

Two cDNA sequences encoding PKC-ι have been deposited, P41743 in Swiss-Prot and Q8WW06 in TrEMBL, and their sequences differed at three positions (L476M, H499L and P551R). The latter sequence was used to obtain the previous structure, although it appeared to be a minor gene given its tissue distribution and number of depositions. Therefore, in addition to the sequence of Q8WW06 in TrEMBL (termed the minor type in this report), constructs from the sequence of P41743 in Swiss-Prot (termed the major type in this report) were tried. The previous structure had 16 and eight disordered residues at the N- and C-termini, respectively. Therefore, in addition to the cDNA for the original length encoding residues 224–587, a cDNA for residues 240–579 (without the disordered regions at both ends) was tried. By combining these two strategies, four expression constructs for the PKC-ι kinase domain were prepared. The sequences of the N-terminal His tag and the TEV protease site were not changed.

These four proteins were expressed and purified by affinity and anion-exchange chromatography. The expression levels and phosphorylation states of the four constructs were investigated after these procedures. Interestingly, the major-type proteins were expressed at a level that was a few-fold higher than the minor-type proteins. Another interesting feature was the phosphorylation level of Thr403 in the activation loop. Western blotting using a phospho-specific antibody for the Thr403 region showed that the phosphorylation level at Thr403 in the major-type protein was lower than that

Table 3
Characteristic interaction of ATP with PKC-ι and corresponding interaction with PKA (PDB code 1atp).

The region names of PKC-ι are indicated.

	ATP	PKC-ι	PKA (1atp)	Region name
Adenine	N6	Glu324 O	Glu121 O	Hinge region
Adenine	N1	Val326 N	Val123 N	Hinge region
Phosphate	O1α	Lys274 N$^{\eta}$	Lys72 N$^{\eta}$	Conserved lysine
Phosphate	O1β	Lys274 N$^{\eta}$	Lys72 N$^{\eta}$	Conserved lysine
Phosphate	O2β	Ser255 N	—	Glycine-rich loop
Phosphate	O2β	Tyr256 N	Phe54 N	Glycine-rich loop
Phosphate	O2β	Ala257 N	Gly55 N	Glycine-rich loop
Phosphate	O3γ	Ser255 N	Ser53 N	Glycine-rich loop
Phosphate	O2γ	Asp387 O$^{\delta2}$	Asp184 O$^{\delta2}$	DFG motif
Adenine	N3	Phe543 C$^{\varepsilon1}$	Phe327 C$^{\varepsilon1}$	C-terminal tail

of the minor-type protein. These results suggested that the expression level of the major-type protein overwhelms the kinase(s) in Sf9 cells, leading to the accumulation of a species lacking Thr403 phosphorylation.

PDK1 is known to phosphorylate Thr in the activation loop of many AGC kinases, such as PKC-ζ (Chou *et al.*, 1998) and AKT (Yang *et al.*, 2002). For phosphorylation of Thr403 in the activation loop *in vitro*, a shorter construct of the major-type protein was incubated with PDK1 and ATP. After this incubation process, a chromatogram from the anion-exchange column (MonoQ) showed that the major peak before incubation disappeared and that the intensity of a minor peak with a longer retention time increased. This result suggests that the anionic character of the protein surface increased after this incubation process. Electrospray mass spectrometry showed that the protein after this incubation was a mixture of doubly and triply phosphorylated species (roughly a 70:30 mixture; data not shown).

Crystal screens using commercially available kits established that the PDK1-phosphorylated protein crystallized under many conditions, while no diffracting crystals were obtained from the protein before PDK1 phosphorylation.

3.2. Structure of the ATP complex

3.2.1. Overall structure. The structure of the ATP complex was determined at 2.1 Å resolution. There are two molecules in the asymmetric unit of the crystal and they superpose well on each other. In both molecules residues 446–456 were not observed, as in the case of the BIM1 complex. In addition to these residues, two short regions were not observed in one of the two molecules (residues 283–287 in chain *A* and residues 395–397 in chain *B*), probably because of crystal packing. In order to remove this effect, we will focus the discussion on the identical structure in both molecules.

The overall structure of the ATP complex is almost identical to that of the BIM1 complex. Electron density for the N-terminus (including part of the TEV-cleaved end) and the C-terminus are well observed in both monomers. Phosphorylation of two threonines in the activation loop (Thr403) and the turn motif (Thr555) is clearly defined. The characteristic hydrophobic motif residues of AGC-branch kinases are also observed as in the BIM1 complex. The most important feature in this structure is residues 533–551. These residues are clearly defined in the ATP complex, while the corresponding residues were not observed in the previously determined BIM1 complex. Fig. 1(*a*) shows the overall structure superposed with the electron density for these residues in the C-terminal region.

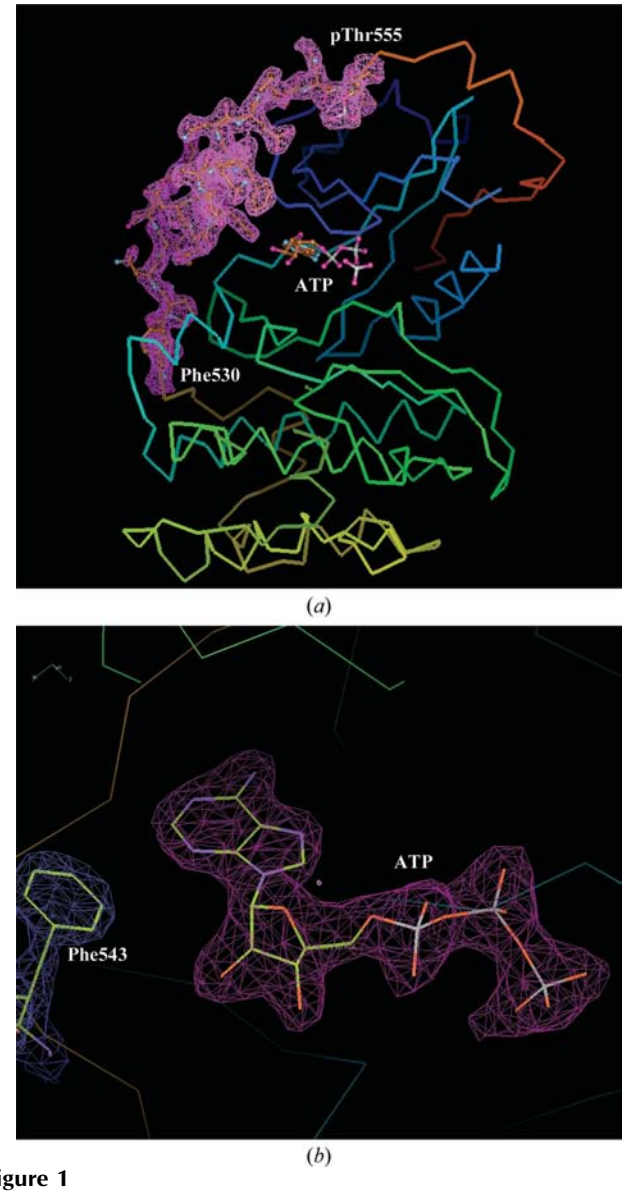

Figure 1
(*a*) Overall structure of the PKC-ι kinase domain in complex with ATP. The $2mF_o - DF_c$ maps for residues 530–555 are superposed in magenta at the 1.3σ level. Protein C$^{\alpha}$ backbone atoms are represented as a rainbow-coloured line, with the N-terminus in blue and the C-terminus in orange. The regions of the small lobe and the large lobe in the kinase core are coloured blue/cyan and cyan/green/yellow, respectively. The C-terminal tail region is coloured brown/orange. The atoms of residues 530–555 and ATP are represented as a ball-and-stick model, with C atoms in gold, N atoms in cyan, O atoms in magenta and P atoms in grey. The electron density of residues 530–555 including the phosphate of Thr555 is clearly observed. (*b*) Structure around ATP. The $2mF_o - DF_c$ maps at the 1.5σ level for ATP and Phe543 are shown in magenta and blue, respectively. The C$^{\alpha}$ backbone of the large lobe, small lobe and linker region between the two lobes are shown in cyan, green and orange, respectively. ATP and Phe543 are shown in coloured lines, with C atoms in yellow, N atoms in purple, O atoms in red and P atoms in grey. The side chain of Phe543 is placed close to ATP.

Table 4
Characteristic interaction between the kinase core/ATP and C-terminal tail residues 533–555.

The region names of the kinase core are indicated.

C-terminal tail	Kinase core/ATP	Region name of kinase core
Phe538 O	Tyr325 O^{η}	Hinge
Phe538 O	Asn327 N^{δ}	—
Asn542 N^{δ}	Asn327 O	—
Phe543 C^{ϵ}	ATP N3	—
Thr548 O	Arg249 N^{ϵ}	—
Glu550 $O^{\delta1,2}$	Arg253 N^{ϵ}, $N^{\eta2}$	Glycine-rich loop
Glu553 O	Lys258 N^{ζ}	Glycine-rich loop
pThr555 O1P	Lys277 N^{ζ}	β3 strand
pThr555 O2P	Arg318 $N^{\eta1}$	β5 strand
pThr555 O3P	Lys258 N^{ζ}	Glycine-rich loop
pThr555 O3P	Arg253 $N^{\eta2}$	Glycine-rich loop
pThr555 O	Arg318 $N^{\eta1}$	β5 strand

The detailed structure, interactions and role of these residues will be discussed later.

3.2.2. Interaction of ATP with the kinase core. As shown in Fig. 1(*b*), electron density for ATP is also clearly observed. Although this crystal does not contain any metals for catalysis or peptide substrates (or their analogues), its binding mode is similar to that of the PKA–Mn-ATP–peptide inhibitor ternary complex (PDB code 1atp) except for the metal-binding site (Johnson *et al.*, 2001). Table 3 summarizes the characteristic interactions between ATP and PKC-ι and the corresponding interactions in the PKA ternary complex. The adenine ring binds the hinge region through two hydrogen bonds. Two O atoms from the α- and β-phosphates make double hydrogen bonds to the side-chain N atom of a conserved lysine (Lys274). These interactions are also observed in the PKA complex.

One O atom of the β-phosphate and main-chain N atoms at the tip of the glycine-rich loop make multiple hydrogen bonds (Fig. 2*a*), which are also conserved in the PKA ternary complex. In the PKA ternary complex the corresponding hydrogen bonds anchor the ATP β-phosphate at the glycine-rich loop to constrain the flexibility of the γ-phosphate so that its position will be suitable for the subsequent phosphoryl transfer. In this PKC-ι–ATP complex, the anchoring of the β-phosphate through multiple hydrogen bonds to the glycine-rich loop is similar to that in the case of PKA, while the direction of the γ-phosphate is different from that in the PKA ternary complex, probably because of the absence of Mg (or its analogue) in the PKC-ι complex. These results suggest that the multiple hydrogen bonds of the ATP β-phosphate to the glycine-rich loop are important interactions and the resulting constraint of the β-phosphate may be one of critical processes in PKC-ι in the path to the activation and transfer of the γ-phosphate.

3.2.3. Structure of the C-terminal tail. As shown in Fig. 1(*a*), residues 533–551 in the ATP complex are clearly defined, while the corresponding residues were not observed in the previously determined PKC-ι–BIM1 complex. This region first wraps around the ATP-binding pocket and then around a small lobe of the kinase core. The characteristic interactions of these residues with the kinase core or ATP are shown in Table 4. The most interesting feature is the interaction of Phe543 with ATP. The side chain of Phe543 is oriented into the ATP-binding pocket to make van der Waals contacts (less than 3.5 Å) with the adenine ring of ATP. This structure is important because (i) this residue interacts directly with ATP, (ii)

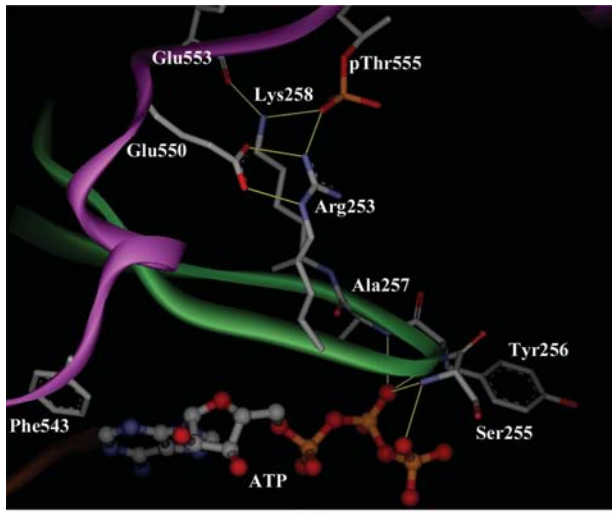

(*a*)

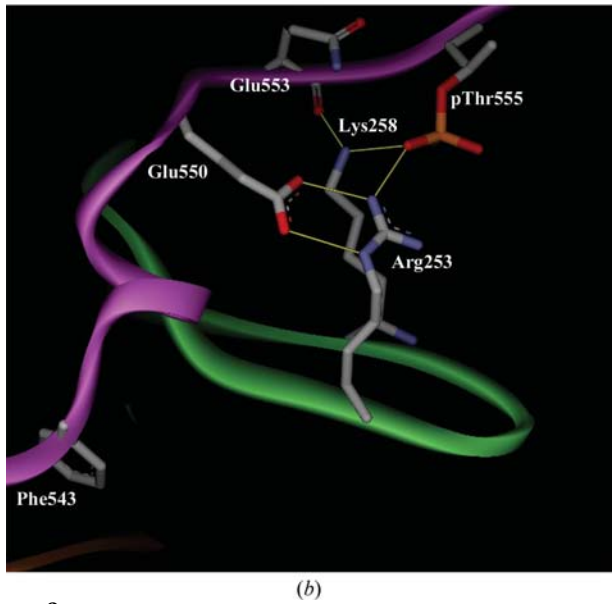

(*b*)

Figure 2
(*a*) Characteristic interaction between the glycine-rich loop and the C-terminal tail in the ATP complex. The protein backbone is rendered as a solid ribbon. The C-terminal tail, small lobe (including the glycine-rich loop) and hinge regions are coloured magenta, green and orange, respectively. ATP is shown in ball-and-stick representation. The residues anchoring the glycine-rich loop or ATP are rendered as sticks. Hydrogen bonds are shown as yellow lines. The side chains of Glu550, the main-chain carbonyl of Glu553 and one O atom of pThr555 make multiple hydrogen bonds to the basic side chains of Arg253 and Lys258 to anchor the glycine-rich loop. The main-chain N atoms of the three residues at the tip of the fixed glycine-rich loop anchor the β-phosphate of ATP, as is the case in the PKA ternary complex. In addition to the hydrogen-bond network, the side chain of Phe543 makes van der Waals interactions to help the binding of ATP. All these interactions promote the binding of ATP cooperatively. (*b*) Corresponding interaction of the apo form. The characteristic interactions are essentially identical to those of the ATP complex. Residues 255–257 are not rendered as sticks because they make no interaction with ATP and because the side-chain conformations of the two monomers in an asymmetric unit are not identical to each other.

this residue is well conserved at the sequence level not only in the PKC family but also in numerous other AGC-branch kinases, (iii) corresponding residues are also oriented into the active site to contact with ligands in the structures of other AGC-branch kinases such as PKA (Johnson *et al.*, 2001) and AKT (Yang *et al.*, 2002) with ATP (or analogues) and (iv) the corresponding residue in PKA is essential for enzymatic activity (Batkin *et al.*, 2000).

Another interesting feature is the multiple hydrogen bonds between the C-terminal tail and the glycine-rich loop (Fig. 2*a*). The side-chain N atoms of Arg253 make multiple hydrogen bonds to the O atoms of the Glu550 side chain and one phosphate O atom of pThr555. Additionally, the side-chain N atom of Lys258 makes hydrogen bonds to the main-chain O atom of Glu553 and the phosphate O atom of pThr555. These multiple hydrogen bonds anchor Arg253 and Lys258 in position. Since these two residues are situated at both sides in the middle of the glycine-rich loop, the restrained structures of Arg253 and Lys258 reduce the flexibility of the glycine-rich loop. As a result, the flexibility of the tip of the glycine-rich loop is reduced and the resulting structure is suitable for binding ATP and forming hydrogen bonds to its β-phosphate, as emphasized in the previous section. In addition to the hydrogen-bond network of these residues, the van der Waals interactions of the Phe543 side chain support the binding of ATP.

These results suggest that the structure and interactions of these newly observed residues in the C-terminal tail are important for ATP binding and activation. These residues were disordered in the previously determined BIM1 complex. When BIM1 is superimposed on the ATP complex, the closest distance between BIM1 and the Phe543 side chain is less than 2.0 Å. It is probable that one of the indolyl rings of BIM1 bumps against the Phe543 side chain, pushing this residue outside the cleft, and the resulting disorder of Phe543 loosens the other interactions between Pro533 and pThr555. A similar effect was observed in PKA. Although all of the C-terminal residues, including Phe327 (Phe543 in PKC-ι), are clearly traced in the structure containing ATP (or ATP analogue), they are not observed in the BIM2 complex.

In other PKC complexes the corresponding C-terminal residues were not observed (PKC–θ-staurosporine) or were traced in only one of two monomers in the asymmetric unit (PKCβII–BIM2), presumably because they have large ligands; the reason for the disorder of these residues may be the same as in the case of the PKC-ι–BIM1 complex.

3.3. Structure of the apo form

The structure of the PKC-ι apo form was determined at 2.0 Å resolution. The crystal form, crystal packing and overall structure of the apo form are essentially identical to those of the ATP complex, although its crystallization conditions were different. Residues 450–456 in the two monomers and additional regions (282–285 and 448–449) are not observed in monomer *B*, a result similar to that obtained for the ATP complex. Two phosphates from threonines in the activation loop and turn motif and characteristic HM residues are also defined as clearly as in the ATP complex.

The situation regarding the C-terminal tail region differs from that of the prototypical AGC-branch kinase PKA. In the structures of PKA, residues 319–328 (535–544 in PKC-ι) are disordered in the apo form and the degree of ordering of this region is determined by the ligands (Akamine *et al.*, 2003; Johnson *et al.*, 2001). In contrast, all the residues in the C-terminal tail are well defined in the apo form of PKC-ι. In addition, the structure and characteristic interactions of this region are essentially identical to those of the ATP complex (Fig. 2*b*). Although there is no substrate in the apo form, the side chain of Phe543 is clearly observed in the same position as in the ATP complex. The side chains of Arg253 and Lys258 in the glycine-rich loop make multiple hydrogen bonds to the C-terminal tail residues in the same manner, so that their positions are restrained as in the case of the ATP complex. These key structures of the two monomers in an asymmetric unit are essentially identical to each other, although their crystal-packing interactions with neighbouring molecules differ, indicating that these structures are not artefacts of crystal packing.

These results indicate that the structure of the apo form is pre-organized for binding ATP, which differs from the case of the prototypical AGC-branch kinase PKA and the inactive precursors of other PKCs (Cameron *et al.*, 2009).

4. Conclusion

Crystal structures of PKC-ι in the ATP-bound and apo forms were determined at 2.1 and 2.0 Å resolution, respectively. Residues 533–551 in the C-terminal tails, which were disordered in the previously determined BIM1 complex, are clearly defined in both structures. In the ATP complex Phe543 protrudes into the ATP-binding pocket to make van der Waals interactions with the ligand and the residues of the newly observed region make multiple hydrogen bonds to the glycine-rich loop. The resulting constrained loop is suitable for ATP binding and anchoring the ATP β-phosphates, which may be one of the critical processes that is necessary for activation and transfer of the γ-phosphate.

The structure of the PKC-ι apo form is essentially identical to that of the ATP complex. The structure of the C-terminal tail and its interaction with the glycine-rich loop are also identical. These results contrast with those for the prototypical AGC-branch kinase PKA, the structure of which changes according to the binding of substrates.

These findings provide new insights into the formation of an ATP-binding pocket within PKC-ι.

References

Akamine, P., Madhusudan, Wu, J., Xuong, N.-H., Ten Eyck, L. F. & Taylor, S. S. (2003). *J. Mol. Biol.* **327**, 159–171.

Batkin, M., Schvartz, I. & Shaltiel, S. (2000). *Biochemistry*, **39**, 5366–5373.

Cameron, A. J., Escribano, C., Saurin, A. T., Kostelecky, B. & Parker, P. J. (2009). *Nature Struct. Mol. Biol.* **16**, 624–630.
Chou, M. M., Hou, W., Johnson, J., Graham, L. K., Lee, M. H., Chen, C.-S., Newton, A. C., Schaffhausen, B. S. & Toker, A. (1998). *Curr. Biol.* **8**, 1069–1077.
Emsley, P. & Cowtan, K. (2004). *Acta Cryst.* D**60**, 2126–2132.
Gold, M. G., Barford, D. & Komander, D. (2006). *Curr. Opin. Struct. Biol.* **16**, 693–701.
Grodsky, N., Li, Y., Bouzida, D., Love, R., Jensen, J., Nodes, B., Nonomiya, J. & Grant, S. (2006). *Biochemistry*, **45**, 13970–13981.
Gustafson, W. C., Ray, S., Jamieson, L., Thompson, E. A., Brasier, A. R. & Fields, A. P. (2004). *J. Biol. Chem.* **279**, 9400–9408.
Johnson, D. A., Akamine, P., Radzio-Andzelm, E., Madhusudan & Taylor, S. S. (2001). *Chem. Rev.* **101**, 2243–2270.
Manning, G., Whyte, D. B., Martinez, R., Hunter, T. & Sudarsanam, S. (2002). *Science*, **298**, 1912–1934.
McCoy, A. J., Grosse-Kunstleve, R. W., Storoni, L. C. & Read, R. J. (2005). *Acta Cryst.* D**61**, 458–464.
Messerschmidt, A., Macieira, S., Velarde, M., Bädeker, M., Benda, C., Jestel, A., Brandstetter, H., Neuefeind, T. & Blaesse, M. (2005). *J. Mol. Biol.* **352**, 918–931.
Moscat, J. & Diaz-Meco, M. T. (2000). *EMBO Rep.* **1**, 399–403.
Murshudov, G. N., Vagin, A. A. & Dodson, E. J. (1997). *Acta Cryst.* D**53**, 240–255.
Tan, S. L. & Parker, P. J. (2003). *Biochem. J.* **376**, 545–552.
Taylor, S. S., Yang, J., Wu, J., Haste, N. M., Radzio-Andzelm, E. & Anand, G. (2004). *Biochim. Biophys. Acta*, **1697**, 259–269.
Xu, Z. B., Chaudhary, D., Olland, S., Wolfrom, S., Czerwinski, R., Malakian, K., Lin, L., Stahl, M. L., McCarthy, D. J., Benander, C., Fitz, L., Greco, R., Somers, W. S. & Mosyak, L. (2004). *J. Biol. Chem.* **279**, 50401–50409.
Yang, J., Cron, P., Good, V. M., Thompson, V., Hemmings, B. A. & Barford, D. (2002). *Nature Struct. Biol.* **9**, 940–944.